Journal of Magnetic Resonance 210 (2011) 218–227

Contents lists available at ScienceDirect

Journal of Magnetic Resonance

journal homepage: www.elsevier.com/locate/jmr

Software compensation of Eddy current fields in multislice high order dynamic shimming

Saikat Sengupta [a,b,*], Malcolm J. Avison [a,c], John C. Gore [a,b,c], E. Brian Welch [a,c]

[a] Vanderbilt University Institute of Imaging Science, Vanderbilt University, Nashville, TN 37235, USA
[b] Department of Biomedical Engineering, Vanderbilt University, Nashville, TN 37235, USA
[c] Department of Radiology and Radiological Sciences, Vanderbilt University, Nashville, TN 37235, USA

ARTICLE INFO

Article history:
Received 7 December 2010
Revised 3 March 2011
Available online 8 March 2011

Keywords:
Dynamic shimming
High field
Eddy currents
Eddy current compensation

ABSTRACT

Dynamic B_0 shimming (DS) can produce better field homogeneity than static global shimming by dynamically updating slicewise shim values in a multislice acquisition. The performance of DS however is limited by eddy current fields produced by the switching of 2nd and 3rd order unshielded shims. In this work, we present a novel method of eddy field compensation (EFC) applied to higher order shim induced eddy current fields in multislice DS. This method does not require shim shielding, extra hardware for eddy current compensation or subject specific prescanning. The interactions between shim harmonics are modeled assuming steady state of the medium and long time constant, cross and self term eddy fields in a DS experiment and 'correction factors' characterizing the entire set of shim interactions are derived. The correction factors for a given time between shim switches are shown to be invariable with object scanned, shim switching pattern and actual shim values, allowing for their generalized prospective use. Phantom and human head, 2nd and 3rd order DS experiments performed without any hardware eddy current compensation using the technique show large reductions in field gradients and offsets leading to significant improvements in image quality. This method holds promise as an alternative to expensive hardware based eddy current compensation required in 2nd and 3rd order DS.

1. Introduction

Dynamic shimming (DS) is a technique for obtaining optimal B_0 field homogeneity during an MR acquisition by updating the shim coil currents for the volume under examination during the scan [1–8]. In DS, multiple shim settings individually optimal for each slice or sub-volume are applied during scanning, leading to better localized compensation of field inhomogeneities than obtained with a single static global shim set that is optimal for the entire volume. The need for specialized hardware has limited the widespread use of DS. However, with increasing field strengths and consequently higher susceptibility artifacts, DS could potentially be an important tool in the future to improve image quality vis-à-vis conventional static shimming techniques.

Most current clinical imaging systems do not permit fast, accurate updating of shim coil currents. Also, most current scanner software do not include real time control of the higher order shims, making it difficult to update shim values dynamically during a scan. In order to overcome these difficulties, all implementations of DS to date have incorporated additional hardware and interfaces for fast updating of the shims [1–6].

The performance of DS may be severely limited by eddy currents and resulting eddy fields produced by the switching of 2nd and 3rd order unshielded shims. These eddy currents flow in the conducting structures of the magnet and cause severe field deviations leading to signal losses, distortion and ghosting in imaging. Also, these fields are time varying and decay with multiple time constants ranging from milliseconds to several seconds [3–5]. Traditionally, eddy current effects produced by first order gradient switching have been minimized by shielded gradient designs [9] and residual eddy current effects compensated by using shaped current waveforms in the gradients [10,11]. These approaches, when extended to shim gradients require extensive hardware additions that are typically not available for higher order shims. Furthermore, compensation of 1st order eddy fields may potentially involve complicated adjustments to the gradient current drives and existing gradient eddy current compensation (ECC) systems.

De Graaf et al. in 2003 developed an analog $Z2$–$Z0$ compensation unit to correct for the $Z0$ eddy fields produced by the unshielded $Z2$ shim coil switching [3]. Koch et al. [4] extended this to include all the 2nd order shim eddy currents. However, the

* Corresponding author. Address: Vanderbilt University Institute of Imaging Science, 1161 21st Avenue South Medical Center North, AA-1105 Nashville, TN 37232-2310, USA. Fax: +1 615 322 0734.
E-mail addresses: saikat.sengupta@vanderbilt.edu (S. Sengupta), calum.avison@vanderbilt.edu (M.J. Avison), john.gore@vanderbilt.edu (J.C. Gore), edward.b.welch@vanderbilt.edu (E. Brian Welch).

1090-7807/$ - see front matter © 2011 Elsevier Inc. All rights reserved.
doi:10.1016/j.jmr.2011.03.007

inclusion of pre-emphasis on the shims reduced the available shim strengths considerably (up to 75% for the $Z2$ shim) [4]. This may not be an option for the already weak 3rd order shims and for potential higher order shims. Eddy current compensation in DS has recently been extended to include 3rd order shims [5]. However, the compensation for all the higher order shims i.e. five second order, seven third order channels, numerous cross terms and additional $Z0$ channels using time constant circuits required highly complex and expensive hardware and calibration. These additional hardware requirements over and above the basic dynamic shim switching hardware can severely limit the universal acceptance of higher order dynamic shimming.

Some scanners now include certain shims that are actively shielded, most commonly the $Z2$ shim. Although this helps in mitigating the eddy current problem, actively shielded shims still require compensation. More often than not, only one or two shims have such active shielding. Active shielding of shims also requires additional hardware that includes the outer shield coil that takes up bore space, separate control boards similar to those of the first order gradients, dedicated communication channels and software controls for precise dynamic operation of the actively shielded coils. Finally, active shielding also reduces the available strength of the shim coil. Overall, hardware based compensation of higher order shim induced eddy currents by either method can prove to be complicated, inefficient and very expensive.

In this work, we present a novel method of software based prospective eddy field compensation (EFC) applied to higher order multislice DS. The technique is independent of the object scanned, slicewise shim amplitude and dynamic shim switching pattern. The method requires only the basic real time shim switching hardware additions. It does not require the use of additional hardware for ECC for the shims or shim shielding and is based on an assumption of reaching an eddy field steady state during an imaging sequence. This method requires a single one time calibration scan that characterizes the eddy field behavior of the shim system and derives *correction factors* that are then used to prospectively correct for the eddy fields produced during any DS acquisition.

2. Theory

Eddy current fields generated by shim switching have been characterized earlier [4,5,12,13]. The 2nd order shims produce strong self and zeroth order eddy fields while the 3rd order shims are seen to produce self, zeroth and very strong first order fields. For example, the $Z2$ shim couples to $Z0$, $Z2X$ shim couples to X and $Z2Y$ shim couples to Y. These fields have large decay time constants of up to a few seconds and superimpose on the existing static field interactions. Dynamic higher order shimming using unshielded shim coils has been shown to be unfeasible when ECC is not used [3–5,12,13].

2.1. Steady state prospective Eddy field compensation

For our method of higher order shim EFC, we make three assumptions. First, we assume that in a multislice DS Gradient Recalled Echo (GRE) experiment, the time varying eddy fields reach a steady state in which the magnitudes of these fields do not change from shot to shot for the same slice. This is a reasonable assumption in a DS multislice GRE experiment where the same set of shim values are applied cyclically and switched at a fixed time interval (which is usually the repetition time (TR)/number of slices), irrespective of the actual slice order. In other words, we assume the system to be reproducible from TR to TR, or to be stationary and linear. Secondly, we assume that the eddy fields produced depend not only on the most recent switch of higher order shim but also on the previous switches. Thirdly, we ignore any change in eddy field magnitude during the GRE data readout window. Given the high sampling bandwidths in GRE imaging and relatively long time constants of the higher order shim eddy currents, this is also reasonable. It follows then, that in an n slice DS experiment we can write:

$$\begin{bmatrix} Ge_1 \\ Ge_2 \\ . \\ . \\ Ge_n \end{bmatrix} = \begin{bmatrix} \Delta G_{1n} & \Delta G_{n,n-1} & \Delta G_{n-1,n-2} & \cdot & \Delta G_{3,2} \\ \Delta G_{2,1} & \Delta G_{1,n} & \cdot & \cdot & \Delta G_{4,3} \\ \cdot & \cdot & \cdot & \cdot & \cdot \\ \cdot & \cdot & \cdot & \cdot & \cdot \\ \Delta G_{n,n-1} & \cdot & \cdot & \cdot & \Delta G_{2,1} \end{bmatrix} \begin{bmatrix} C_1 \\ C_2 \\ . \\ . \\ C_{n-1} \end{bmatrix} \quad (1)$$

or

$$Ge = \Delta G \cdot C \quad \& \quad [(\Delta G^T \Delta G)^{-1} \Delta G^T] \cdot Ge = C \quad (2)$$

Here, $\boldsymbol{Ge}$ is the $n \times 1$ vector of an eddy field harmonic prevalent during individual slice acquisitions. We identify $\boldsymbol{Ge_i}$ as the deviation of a field harmonic magnitude from its ideal value for slice i due to the eddy field. The harmonic represented in $\boldsymbol{Ge}$ may be the same as the switched shim (self interaction) or different (cross term). $\boldsymbol{\Delta G}$ is a $n \times n-1$ matrix of the slicewise shim differences such that $\Delta G_{ij} = G_i - G_j$ where G_i is the shim setting for slice i and $\boldsymbol{C}$ is a $n-1$ element vector of *correction factors* which gives the contributions of the $n-1$ recent shim switches to the eddy field of any harmonic prevailing during acquisition of any slice. Therefore, in a regular multislice DS GRE experiment where shim values are updated in every slice, $\boldsymbol{C}_1$ is the contribution of the most recent shim switch to the eddy field in any slice i given by $\boldsymbol{Ge}_i$, $\boldsymbol{C}_2$ is the contribution of the next most recent shim switch and so on.

Eddy currents are generated in conducting structures placed in the vicinity of time varying magnetic fields such as those generated by dynamically switched shims. By Faraday's law, the magnitude of the currents will depend on the rate of change of the magnetic field and the geometry and impedance of the shim coils and conducting structures. Also, the time constants with which the eddy currents in the conducting structures decay depend on the physical properties of the structures, such as their impedance and temperature, with the resistive component of the impedance being closely related to the temperature. Generally, the lower the temperature of the structure, the longer it takes for the currents to decay. Therefore, the eddy currents and hence the eddy fields produced in the magnet for any particular shim switching pattern remains the same regardless of the object imaged, provided the above physical conditions remain the same. Furthermore, since the correction factor vectors $\boldsymbol{C}$ specify only the relative contributions of the recent shim switches to the eddy field, $\boldsymbol{C}$ is also independent of the actual shim amplitudes.

$\boldsymbol{C}$ may be estimated for the eddy interaction between any pair of shim harmonics by using just a one time calibration scan. For example, the time varying $Z0$ field produced by $Z2$ shim switching yields a vector for the $Z2$–$Z0$ interaction denoted as C_{Z2}^{Z0}, which remains invariant with varying shim switching patterns, amplitudes, slice geometry and imaged object, for a fixed time between shim switches (Δt_{ss}) and number of shim switches. Therefore, for that particular Δt_{ss}, $\boldsymbol{C}$ can be used to calculate the eddy fields expected for the given $\boldsymbol{\Delta G}$ to prospectively compensate for the eddy fields, assuming that the structures in the magnet in which the eddy currents flow and their relevant properties remain the same. Therefore, a complete one time calibration of all the shim eddy interactions for a particular multislice DS experiment parameterized only by Δt_{ss} yields a set of $\boldsymbol{C}$ vectors which can compensate for all eddy fields without the use of any hardware eddy current

compensation. For a standard higher order shim system with 12 higher order shims and 16 channels in all (including X, Y, Z and $Z0$) for example, the entire matrix of correction factors including self and cross terms would be an $n-1 \times 16 \times 16$ array. $\Delta \boldsymbol{G}$ is then a $n \times n-1 \times 16$ matrix representing the shim switching of all the 16 shims and $\boldsymbol{Ge}$ is an $n \times 16 \times 16$ array representing the slicewise eddy fields due to all the shim interactions. Summing $\boldsymbol{Ge}$ in the 3rd dimension gives the total eddy field in any harmonic for every slice.

The above formulation can be extended to a range of Δt_{ss} and slices to yield $\boldsymbol{C}$ vectors for a complete generalized solution. For larger Δt_{ss}, the eddy currents due to a particular shim switch may decay away before the next switch and acquisition. Therefore, the contributions to the eddy field at any slice from the less recent switches may decrease. Also, as the number of slices change for a particular Δt_{ss}, the steady state is set up differently which results in different correction factors.

In the following sections, we present evidence of the invariability of $\boldsymbol{C}$ to various experimental parameters including the sample, the actual shim switching pattern and shim values. The $\boldsymbol{C}$ vectors derived from phantom calibration scans are applied in phantom and human DS experiments. Results from 2nd and 3rd order multislice GRE as well as single shot echo planar imaging (EPI) DS experiments performed on phantom and humans without the use of any hardware based higher order eddy current compensation or shim shielding are presented.

3. Methods

All studies were performed on a 7 Tesla whole body human MRI system (Philips Healthcare Inc., Cleveland Ohio, USA) based on a Magnex 90 cm bore magnet (Magnex Scientific Ltd., Yarnton, Oxfordshire, UK) with a 16 channel SENSE array receiver coil and a single channel quadrature transmit volume coil (Nova Medical, Inc., Wilmington, MA, USA). The scanner employs 14 shim amplifiers (Resonance Research Inc., RRI, Billerica, MA, USA, M*X*H −14, ±10 A, Full power bandwidth: DC – 35 kHz, Full scale rise time 10–90%: 1 ms). Each of the amplifiers has an additional auxiliary analog input for separate additive shim drive control. The system design includes seven unshielded 3rd order shims ($Z3$, $Z2X$, $Z2Y$, $Z(X2–Y2)$, XYZ, $X3$, $Y3$), five unshielded 2nd order shims ($Z2$, ZX, ZY, $X2–Y2$, XY), two actively shielded shims ($Z2$Dynamic or $Z2$D, $Z0$) and shielded first order imaging gradients.

A tool to calculate slicewise fieldmap-based shims up to 3rd order was developed in Matlab (TM)2008a (Mathworks Inc., Natick, MA, USA) with a graphical user interface (GUI) that was run on the MR scanner's console computer. First-order shimming was provided via the three actively shielded 1st order gradients, controlled by the scanner's imaging gradient amplifiers. Slicewise storage and dynamic update of 2nd and 3rd order shims was performed using a separate shim control hardware module. (RRI's '*Load & Go Real Time Shims RTS*' M*X*V 14/4). The GUI on the console computer communicated with the RTS via an RS232 serial connection. The module was connected to the auxiliary input of the shim unit via an analog connection. The RTS module had no built-in ECC mechanism. Therefore, severe eddy fields were expected in a higher order multislice DS experiment.

A complete static shim calibration up to 3rd order was performed using a 17 cm spherical doped water braino phantom placed at magnet isocenter. Individual shims were stepped in the full range of the rated current output of the shim amplifiers in steps of 20% (2 Amps) and multislice axial fieldmaps were obtained. A reference fieldmap obtained without any shim applied was subtracted from these fieldmaps and the resulting maps were fit to the set of spatial shim harmonic functions using a multilinear least squares regression function. A set of shim calibration coefficients were hence obtained, specifying the field in $(\mathrm{mT/m^n})$/Ampere of shim current, n being the order of the shim, as well as the static cross term interactions between the shims in units of $(\mathrm{mT/m^{n'}})/(\mathrm{mT/m^n})$, where n' is the order of the cross term shim harmonic produced. These coefficients were used in our studies to calculate the shim currents. In the DS experiments, slicewise shims were calculated using a multiple linear least squares fitting routine on fieldmap data and input into the RTS. The shim degeneracy analysis presented by Koch et al. [4] was included in the shim calculations. During the scan, shim values from the RTS were applied synchronously with trigger from the spectrometer running the pulse sequence. A time delay of 5 ms was added after the shim switch and before the excitation pulse to allow for current settling of the shim amplifiers.

3.1. Calibration scans and invariability of correction factors

Calibration scans were performed on the shim system to obtain $\boldsymbol{C}$ vectors for all eddy field interactions at a Δt_{ss} = of 18.7 ms and also to test for invariability of $\boldsymbol{C}$ with the sample, actual shim values and switching pattern. The scans were performed on different days on two different phantoms, a 17 cm diameter spherical doped water "braino" phantom and a copper sulphate human head shaped phantom. Multislice GRE DS fieldmapping experiments were performed with a ΔTE of 1 ms. Individual 2nd and 3rd order shims were switched in different arbitrary patterns for nine slice (Fig. 1a: 4 $Z2Y$ shim patterns, 3 in head phantom, 1 in spherical phantom; 1 $Z2X$ pattern, TR/first TE/ΔTE = 168.0/4.4/1.0 ms, slice thickness/gap = 2/2 mm) and 25 slice (Fig. 1b: three unshielded $Z2$ patterns, spherical phantom, TR/first TE/ΔTE = 467.0/4.4/1.0 ms, slice thickness/gap = 2/2 mm) axial scans. All other shims were set to 0. Reference fieldmaps acquired without any shims applied were subtracted from the above fieldmaps. The $Z0$ offsets expected due to slice positions were also subtracted. Shim decomposition up to 3rd order was performed to identify the harmonics that correlated strongly with the switched shim pattern (cutoff r^2 = 0.9). The slicewise coefficients of the relevant harmonics were then used as $\boldsymbol{Ge}$ in Eq. (2) to calculate initial $\boldsymbol{C}$ vectors. These initial $\boldsymbol{C}$ vectors for each particular interaction, for example, C^{Y}_{Z2Y} i.e. changes in the Y shim due to switching of $Z2Y$, obtained from different calibration scans were averaged and fit to a second order polynomial to yield the final $\boldsymbol{C}$ vectors.

For calculating the $\boldsymbol{C}$ vectors for the 'self' shim interactions, i.e. the eddy fields in the shim harmonic that is switched, the 2nd order shims (unshielded $Z2$, shielded $Z2$, ZX, ZY, $X2Y2$ and XY) were switched individually in 25 slice axial GRE head phantom fieldmapping scans with the second switching pattern shown in Fig. 1b (or its inverse). The applied shim values, i.e. the intended fields were subtracted from the actual values obtained for that harmonic from fieldmap shim decomposition. This yielded the field deviation from ideal which we attributed to the eddy current fields. These slicewise additional fields were then used as $\boldsymbol{Ge}$ in calculating $\boldsymbol{C}$ for these interactions.

In this manner, the entire $n-1 \times 16 \times 16$ correction factor matrix describing the interactions for whole shim system for a particular Δt_{ss} (18.7 ms) was populated.

3.2. Generalization to varying Δt_{ss} and number of slices

The eddy field correction procedure described here is based on the assumptions of steady state conditions set up by rapid cyclic shim switching. Therefore, Δt_{ss} and number of slices or shim switches per cycle are parameters that determine the $\boldsymbol{C}$ vectors. To investigate the variation of the $\boldsymbol{C}$ vectors with Δt_{ss} and the number of slices, two sets of scans were performed. The first experi-

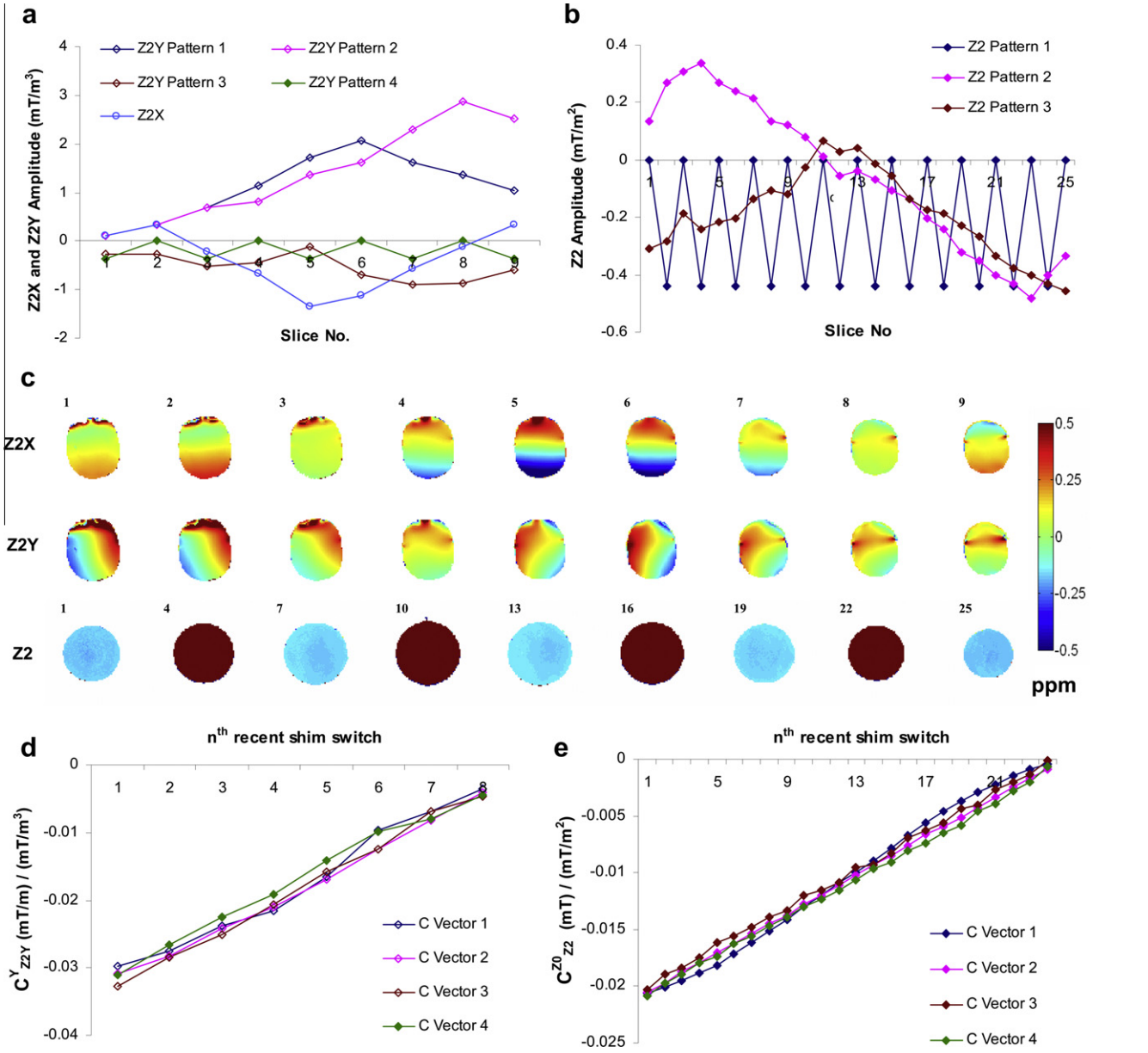

Fig. 1. Calibration of eddy fields and correction factor reproducibility. (a) Switching of *Z2X* and *Z2Y* shims. (b) 25 slice switching patterns of unshielded *Z2* shim in a spherical phantom. Solid markers indicate spherical phantom, open markers indicate head phantom. (c) Fieldmaps acquired using the shim switching patterns shown in a and b after reference subtraction, showing eddy fields. Top and middle rows shows head phantom fieldmaps obtained from switching *Z2X* and *Z2Y* (pattern 1) shims (*x* axis was vertical). All slices show large *X* and *Y* field gradients, which significantly exceed gradients expected from only static *Z2X* to *X* or *Z2Y* to *Y* interactions. Bottom row shows spherical phantom fieldmaps obtained by switching the unshielded *Z2* (pattern 2). Field offsets for the slices where *Z2* was 0 are not equal to 0 ppm. Slice numbers are shown on upper left. (d) 9 slice C^{Y}_{Z2Y} vectors obtained from the 4 *Z2Y* switching patterns shown in a (e) 25 slice C^{Z0}_{Z2} vectors obtained from switching patterns of unshielded *Z2* shim in shown in b. Pattern 2 of b was repeated on a different day, yielding C^{Z0}_{Z2} vector 4.

ment probed the variation of **C**, specifically C^{Z0}_{Z2} with changing Δt_{ss}. Nine slice axial GRE fieldmaps scans were performed using the spherical phantom with only the unshielded *Z2* shim switched in the switching pattern = 0, −0.4, 0, −0.4, 0, −0.4, 0, −0.4, 0 mT/m^2 for a range of TRs (TR/Δt_{ss} = 168/19, 250/28, 500/55, 750/83, 1000/111, 2000/222, 5000/555, 10000/1111, 15000/1666, 25000/2778, 40000/4444 ms). The fieldmaps were analyzed as described above and C^{Z0}_{Z2} vectors obtained for each of the Δt_{ss}. In the second set of scans, only the *Z2X* shim was switched between 0 and −0.37 mT/m^3 (1 Amp) for alternate slices of GRE field mapping scans with the head phantom. The scans were repeated for 5, 8, 9, 11, 15 and 25 slices. The Δt_{ss} was 18.7 ms for all the scans. C^{X}_{Z2X} for all the scans was obtained from the fieldmaps acquired using the same procedure.

3.3. Correction scans

3.3.1. Phantoms

To validate the 'self' channel correction, the calibration scan experiment was repeated. The 'self' ***C*** vectors were now used to calculate the field deviations expected due to the eddy fields using Eq. (1) and prospectively adjust the individual shims. The shielded *Z2* shim was not adjusted as it compensated intrinsically for the self eddy fields produced and hence served as a reference for comparing the performance of the unshielded *Z2* coil with and without correction.

For validation of the correction technique for complete 2nd and 3rd order DS, 9 and 25 slice low resolution fieldmaps were obtained for the spherical and head phantoms. The imaging parame-

ters were the same as above, but with all shim currents set to 0 Amps. Using a region of interest (ROI) defined by all voxels with nonzero signal in every slice, slicewise shim values up to 2nd order (for the spherical phantom) and 3rd order (for the head phantom) were calculated. The slicewise shim eddy field corrections for all the shim channels were obtained using the complete correction factor matrix derived from the calibration scans and prospectively added to the shim values. Dynamically shimmed GRE based fieldmaps were then acquired at 128 × 128 pixel resolution with and without the eddy field corrections at a Δt_{ss} of 18.7 ms, which matched the Δt_{ss} of the calibration scans.

3.3.2. Humans

All human volunteers provided informed written consent and were scanned under an IRB approved protocol. For the human scans, low resolution human head fieldmaps ($n = 4$ subjects, 64 × 64 pixels, 25 slices, TR/first TE/ΔTE = 196.0/3.94/1.0 ms, slice thickness/gap = 3/1 mm) were obtained with all shims zeroed. The fieldmaps were masked using skull stripping and intensity thresholding combined with the operator defined rectangular ROI to delineate the final shim region. Slicewise shim coefficients up to 3rd order were calculated, the corrections applied as described above. Dynamically shimmed GRE images and fieldmaps (128 × 128 pixels, same image geometry as the fieldmaps, TR/first TE/ΔTE/Δt_{ss} = 467.0/4.4/1.0/18.7 ms) were acquired with and without the prospective steady state eddy current corrections. The scans without the eddy field corrections included the static cross term corrections. Importantly, the $\boldsymbol{C}$ vectors used in the human scan corrections were the ones derived from the phantom calibration experiments.

In order to validate the corrections in low bandwidth imaging, single shot gradient echo–echo planar scans were also performed on an individual subject. Twenty-five axial slices were acquired with the same scan geometry as above, with TR/TE = 2765/27 ms and no SENSE acceleration, giving a Δt_{ss} of 110 ms. The scans were performed with 2nd and 3rd order DS, with and without the steady state field corrections. The scans without the eddy field corrections included the static cross term corrections. Ten dummy scans were used to allow the eddy fields to reach a steady state. Care was taken to ensure that the slicewise shim values for each scan were also applied during the echo phase offset determining preparation stage. It was necessary to perform an offline reconstruction to eliminate severe $N/2$ ghost artifacts, most likely caused due to short time constant eddy currents distorting k space sampling. A simple phase correction was performed by extracting the phase difference between the odd and even echoes of the phase calibration preparation scan and multiplying only the odd lines of the actual data set in hybrid k–t space by this difference.

4. Results

Fig. 1c shows fieldmaps obtained from the calibration scans using $Z2X$, $Z2Y$ pattern 1 and $Z2$ shim switching pattern 2, shown in Fig. 1a and b. The head phantom slices show significant 1st order gradients. The interaction between the shims when measured in a static regime are relatively minor (−0.0032 ppm/cm of X per mT/m^3 of $Z2X$ and −0.001 ppm/cm of Y per mT/m^3 of $Z2Y$) compared to these severe gradients observed when the shims are switched dynamically. These significant deviations from the fields that would be expected in a static shimming regime point to strong 1st order eddy fields produced by 3rd order dynamic shim switching i.e. $Z2X$ switching producing X and $Z2Y$ producing Y gradients. In the absence of eddy fields, the spherical phantom fieldmaps would be expected to have slice to slice $Z0$ variations originating only from the *static* $Z2$–$Z0$ interaction. Therefore, the odd numbered slices acquired under a $Z2$ shim value of 0 mT/m^2 would be expected to have no $Z0$ offset. However, a consistent $Z0$ offset is seen on all the odd slices of the spherical phantom, indicating the presence of $Z0$ eddy fields produced by $Z2$ switching which prevent the $Z0$ field value reaching 0 ppm following the $Z2$ switch from −0.4 mT/m^2 to 0 mT/m^2.

4.1. Calibration scans and Invariability of correction factors

Figs. 1d and 1e demonstrate the invariability of the $\boldsymbol{C}$ vectors with the imaged object and the shim switching pattern for a particular Δt_{ss}. Fig. 1d shows four C^{Y}_{Z2Y} vectors obtained from four different calibration scans with the $Z2Y$ shim switching patterns given in Fig. 1a using the spherical (solid markers) and head (open markers) phantoms, showing high reproducibility. Fig. 1e illustrates the C^{Z0}_{Z2} vectors obtained from separate 25 slice calibration scans with different shim switching patterns shown in Fig. 1b. The $\boldsymbol{C}$ vectors show a very high degree of agreement, irrespective of the shim amplitudes, switching patterns, phantom used and day of scanning. The high degree of repeatability in the $\boldsymbol{C}$ vectors observed here is critical to the successful operation of this method.

4.2. Adjustment of $\boldsymbol{C}$ vectors by inclusion of static cross terms

The phantom calibration scans yielded $\boldsymbol{C}$ vectors that described the interaction between any pair of shims. However, the $\boldsymbol{C}$ vectors calculated according to Eq. (2) were observed to predict an estimate of $\boldsymbol{Ge}$ having a constant offset from the actual $\boldsymbol{Ge}$ for all slices. Empirically, this offset was observed to be the *mean value of the switched shim over all the slices multiplied by the static interaction factor* between the relevant pair of shims. Therefore, in steady state, the eddy fields were observed to superimpose on this slicewise static interaction level that was constant for all slices. To account for this offset, an additional unity column was added to $\boldsymbol{\Delta G}$ making it an $n \times n$ element matrix, where n is the number of slices and $\boldsymbol{C}$ was changed to an $n \times 1$ element vector with the final element specifying the value of the static cross term. With this adjustment, the calibration process not only accounted for the time varying eddy fields but also the static cross terms between the shims. These modified $\boldsymbol{C}$ vectors hence produced were used in all our experiments for eddy field compensation including the phantom and human scans described in Section 3.

4.3. Self shim corrections

Fig. 2a–e shows the measured values of the 2nd order shim harmonics (XY, $X2$–$Y2$, ZY, ZX, $Z2$) obtained from the 25 slice spherical phantom scans before and after applying 'self' correction. The prescribed values are also plotted. In the absence of correction, the eddy fields in the self channels prevent the shims from reaching the prescribed level. As a result, incorrect slicewise shim fields are observed. With correction, the fields are adjusted to closely match the slicewise prescribed values. The field errors observed without corrections should not be confused with calibration errors.

4.4. Shielded vs. unshielded Z2 coil

Fig. 2e compares the performance of the shielded $Z2$ coil without correction to the unshielded $Z2$ coil with correction. The shielded $Z2$ coil follows the prescribed field closely, as expected. Without correction, the $Z2$ field from the unshielded $Z2$ coil is severely compromised by the self eddy fields. The initial slices are maximally influenced owing to the largest switch in shim values from the last to the first slice (ascending non interleaved slice order was used). After correction, the slicewise fields agree with the ideal values and the ones produced by the shielded $Z2$ coil Therefore, the

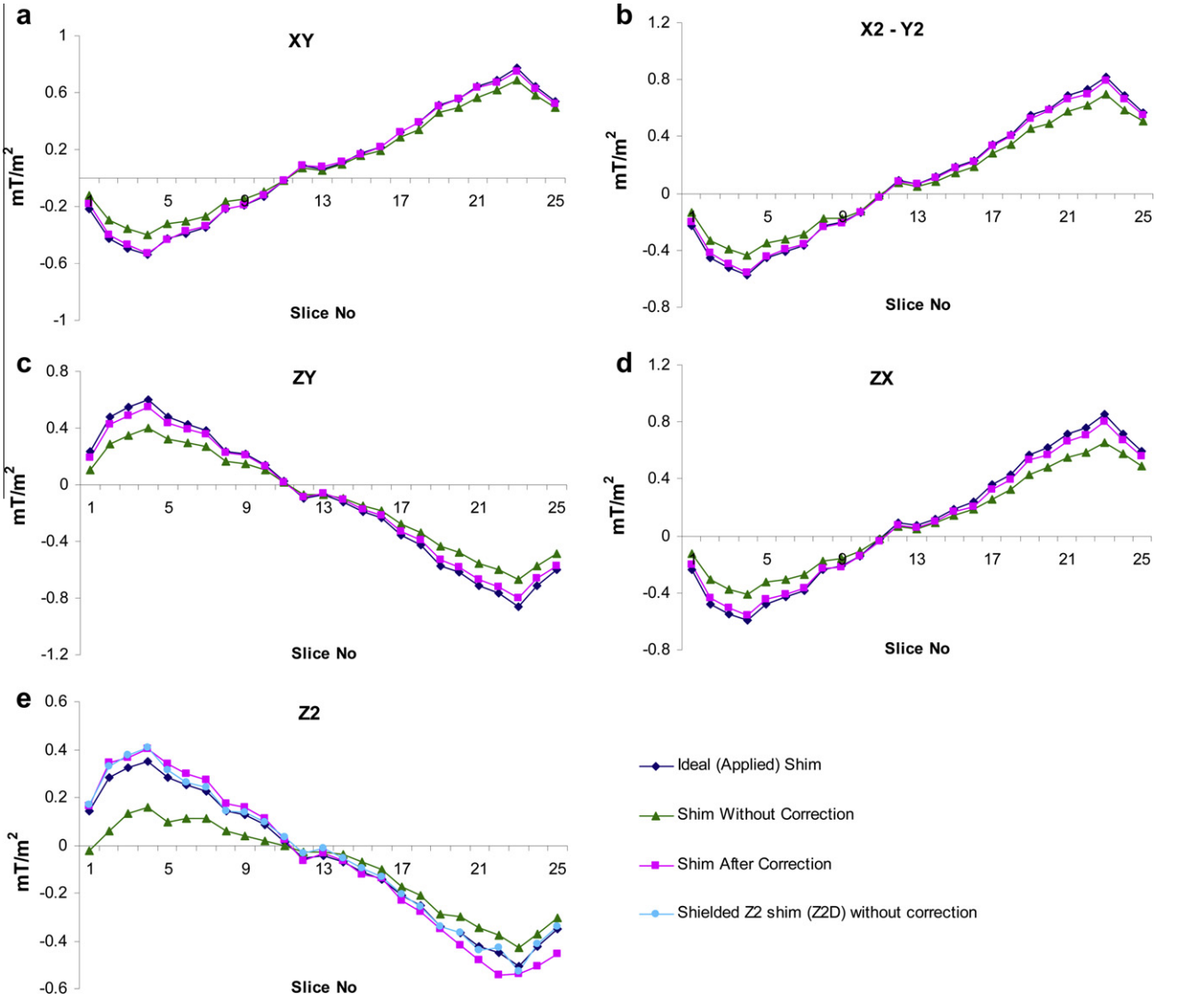

Fig. 2. 2nd order self shim corrections (a–e): *XY*, *X2–Y2*, *ZY*, *ZX*, *Z2* shim values for a 25 slice DS GE experiments with and without self corrections. The corrected fields agree closely with the ideal fields in all the shims. The unshielded *Z2* shim field after correction follows the ideal and the shielded shim field values.

C_{Z2}^{Z0} vector gives us an entirely software based correction for the self eddy field produced by the unshielded, uncompensated *Z2* coil. These results therefore indicate that one may be able to produce unshielded shim coil performance similar to that of a shielded coil very easily by prospectively applying the steady state software based corrections.

4.5. Generalization to varying Δt_{ss} and number of slices

The extension of the method to varying Δt_{ss} is important for its general applicability. Fig. 3a shows the C_{Z2}^{Z0} correction factors obtained from nine slice scans with TRs/Δt_{ss} ranging from a minimum allowed of 168/19 ms to 40.0/4.4 s. The $\boldsymbol{C}$ vectors up to around TR/Δt_{ss} of 2000/222 ms coincide with each other, with subsequent vectors deviating increasingly from the initial cluster. With increasing TR's above 2000 ms, the correction factor values from all the switches except the most recent have decreasing absolute values, indicating progressively declining contributions to the eddy fields from these switches. However, for a large range of commonly employed TRs, the $\boldsymbol{C}$ vectors do not vary significantly and therefore may be successfully used in a range of experiments.

Fig. 3b shows the variation of $\boldsymbol{C}$ vectors with number of slices for the same $\Delta t_{ss.}$ The $\boldsymbol{C}$ vectors change significantly with the number of slices with the *n*th recent switch accounting for lesser amounts of the eddy fields as the number of slices are reduced. The variation in the $\boldsymbol{C}$ vectors reflects the effect of the shim switching cycle period on the steady state field developed.

4.6. Complete shim correction scans: phantoms

Fig. 4 illustrates the corrections obtained in complete 2nd and 3rd order phantom DS experiments. Fig. 4a shows nine axial slice fieldmaps acquired of a spherical phantom using 2nd order DS, with and without eddy field corrections. The fieldmaps without eddy field corrections included conventional static *Z2–Z0* correction of -2.08 ppm/mT/m^2 of *Z2* for all slices. The fieldmaps without the steady state corrections however show residual field offsets that are different for different slices and are not compensated by just the static correction. These offsets caused by eddy fields from *Z2* switching are compensated in the scans with the steady state corrections. The steady state correction includes the static interaction correction as well, which is inherently

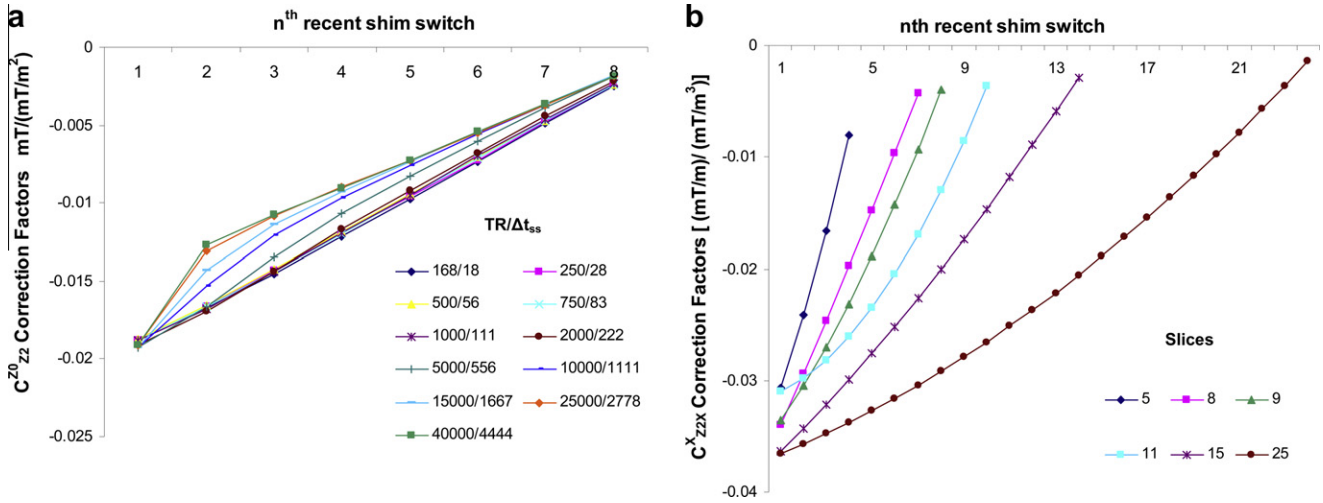

Fig. 3. (a) Change of $\boldsymbol{C}$ with Δt_{ss}. C^{Z0}_{Z2} vectors are shown as an example for nine slice experiments with varying Δt_{ss}. (b) Change of $\boldsymbol{C}$ with number of slices for same Δt_{ss}. C^{X}_{Z2X} vectors are shown as an example for Δt_{ss} = 18.66 ms with varying number of slices.

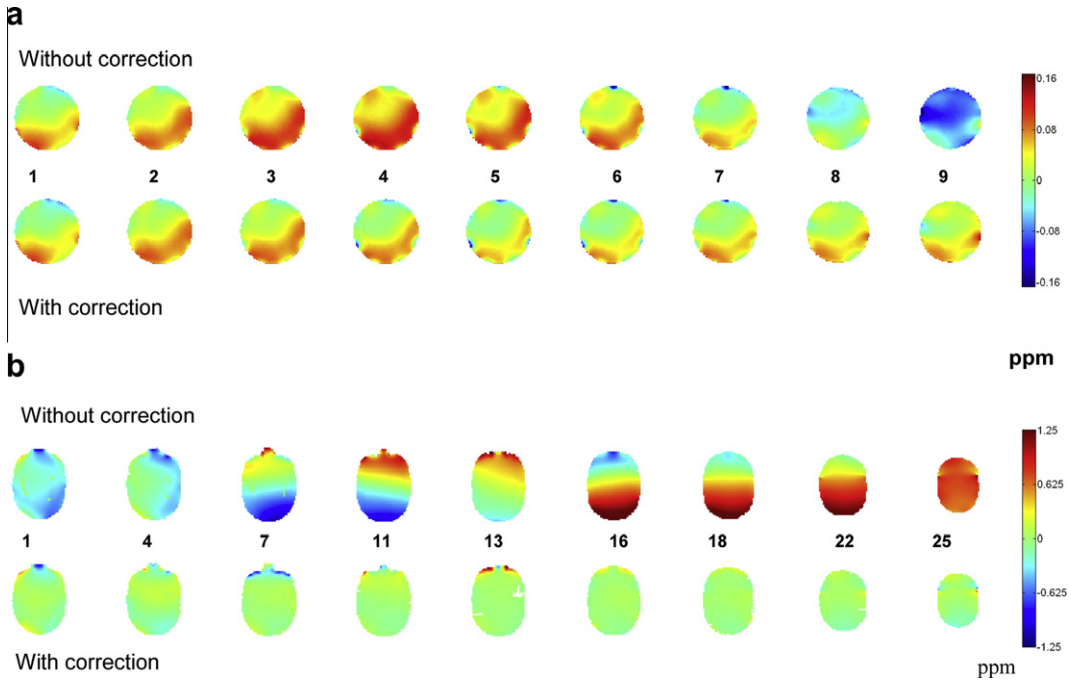

Fig. 4. Correction results from 2nd and 3rd order DS GRE phantom experiments. (a) Fieldmaps in ppm from a 2nd order DS scan, without and with *Z2–Z0* eddy field correction. (b) Fieldmaps from 3rd order DS scan, without and with *Z2X* to *X* and *Z2Y* to *Y* corrections. In all cases severe field offsets and gradients are corrected.

captured in the modified $\boldsymbol{C}$ vector. Fig. 4b shows selected slice fieldmaps from a 25 slice head phantom scan using 3rd order DS. In all slices, severe field gradients caused by 3rd to 1st order eddy field interactions are corrected using this method, without any hardware ECC or individual prescanning. This indicates that 3rd order DS is possible without using hardware ECC or shielded shim coils.

4.7. Correction scans: humans

The $\boldsymbol{C}$ matrix used for the eddy field correction in the human DS experiments was derived entirely from calibration scans run on phantoms. No calibration scans were run on human subjects. Also, the slice gaps and thicknesses used in the human scans (3/1 mm) were different from those used in the phantom calibration scans (2/2 mm).

Fig. 5 shows fieldmaps from 25 slice human head 3rd order DS scans with and without corrections. The fieldmaps without corrections show severe offsets and field gradients due to the eddy currents produced by 2nd and 3rd order shim switching. The magnitude of the field is well in excess of 1 ppm at places, and the *x* and *y* field gradients exceed 0.1 mT/m, which can cause significant pixel displacements even at high readout bandwidth GRE imaging (bandwidth 0.032 mT/pixel here). In comparison, the fieldmaps with the correction show well shimmed fields, with excellent homogeneity. These results strongly suggest that the method is applicable under the higher and more arbitrary slicewise shim correction demands usually encountered in the human brain

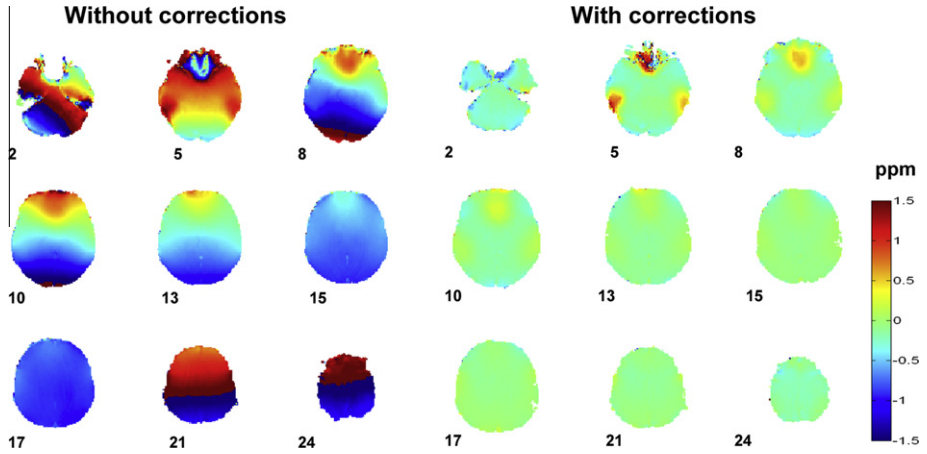

Fig. 5. Selected slice fieldmaps showing results from 3rd order DS GRE human experiments without and with steady state eddy field corrections. In all cases severe field offsets and gradients are corrected by the method. Field wraps are observed in the maps without correction, indicating field offsets greater than 1.7 ppm (1.7 ppm = 500 Hz = 1/2 * 1/ΔTE, ΔTE = 1 ms). Slice numbers indicated below the fieldmaps.

and the ***C*** factors obtained from phantom calibrations are very reliably translatable to human scans.

The single shot echo planar images show considerable improvements with steady state field corrections in both 2nd and 3rd order DS. Selected slices after *N*/2 ghost removal are shown in Fig. 6. The uncorrected 2nd order DS images show bulk shifts in the phase encode (left–right) direction as a result of 2nd order shim to *Z*0 eddy field interactions. These shifts are corrected by the field corrections, indicating the compensation of *Z*0 eddy fields. The 3rd order DS images without correction show very poor quality with large distortions, shifts and signal losses. Significant in-plane skewing as well as stretching distortions are observed and indicate large field gradients in the frequency and phase encode directions. These correlate well with the gradients observed in the fieldmaps, as expected. In some slices (for example in slice 1), signal is lost completely due to eddy fields in the through plane direction. The steady state corrections correct for these effects to a large extent. Distortions, bulk shifts and signal losses are corrected leading to greatly improved image quality. In addition, improvements are also observed in the amount of ghosting in several slices.

5. Discussion

A promising new method for software based prospective compensation of eddy fields produced by shim switching in DS experiments has been described and demonstrated. The method does not require expensive ECC hardware, shim shielding or subject specific prescanning and can greatly reduce eddy current related field perturbations in higher order DS. Being a software based method, this technique has significant potential in speeding the incorporation of dynamic shimming across a wide range of MR techniques using standard MR scanner configurations.

In addition to not requiring any form of compensation hardware or shim coil shielding, the eddy fields are measured from the actual imaging scan. This is in contrast to traditional eddy field measurement techniques, in which only a step response of the shim is measured. As a result, the convolution effects of rapid repeated shim switching are not captured using the traditional methods. Furthermore, other effects like temporal field fluctuations from pulsed gradient coil vibrations which are usually not compensated can also be potentially accounted for using this method, since they may also be assumed to reach a steady state with shim switching. Also, this method does not reduce the dynamic range of the shims, as is often the case in shim shielding or hardware shim waveform shaping [4,5].

The ***C*** vectors derived from the calibration scans have been shown to be fixed over a range of imaged objects including the human head, shim switching patterns and actual shim values. The correction factors translate into a characterization of the long time constant eddy current behavior of the shims and the magnet structure. The modified *n* element ***C*** vectors inherently account for the dynamic eddy fields as well as the static interactions on which the eddy fields superimpose. The last element of the modified ***C*** vector was seen to be equal to the mean value of the switched shim multiplied by the static interaction factor between the two shim harmonics.

The ***C*** vectors have been demonstrated to be largely consistent over a range of TRs. The *Z*2–*Z*0 interaction considered here as a representative example has highly coincident ***C*** vectors up to TRs of at least 2000 ms or Δt_{ss} of 222 ms. As long as the shims are switched in a cyclic manner with a fixed period and Δt_{ss}, we hypothesize the calibration factors will be reproducible irrespective of the sequence type. Results from the EPI scans for example show that even though we introduced the method in the context of GRE scans, the correction procedure is independent of the sequence and is dependent only on Δt_{ss} and number of slices. Most of the commonly employed GRE and EPI based scans have much smaller Δt_{ss} values and therefore, a single ***C*** matrix should be sufficient to compensate for all regular multislice GRE DS scans. This technique should also be applicable to 3D GRE scans, which may be of interest in parcellated DS techniques [8]. For EPI scans commonly used in functional MRI, certain number of dummy scans over the volume may be employed to reach shim steady state, before actual data acquisition. This is not a hindrance as dummy scans are commonly employed in most dynamic echo planar functional experiments. Further work is however needed to evaluate the robustness of the ***C*** vectors with respect to different sequences, especially in long TR scans such as in multislice spectroscopic imaging.

The technique provided excellent compensation of eddy fields in the GRE scans. However even though the 3rd order DS echo planar image quality was improved substantially with the correction, the images still displayed residual distortions. One of the reasons may be the fact that the data acquisition windows of the EPI scans are much longer than those of the GRE scans. As a result, the short time constant eddy fields that decay in the time scale of the acquisition window of EPI do not reach the steady state reached by the medium and long time constant fields. Also, with the inclusion of

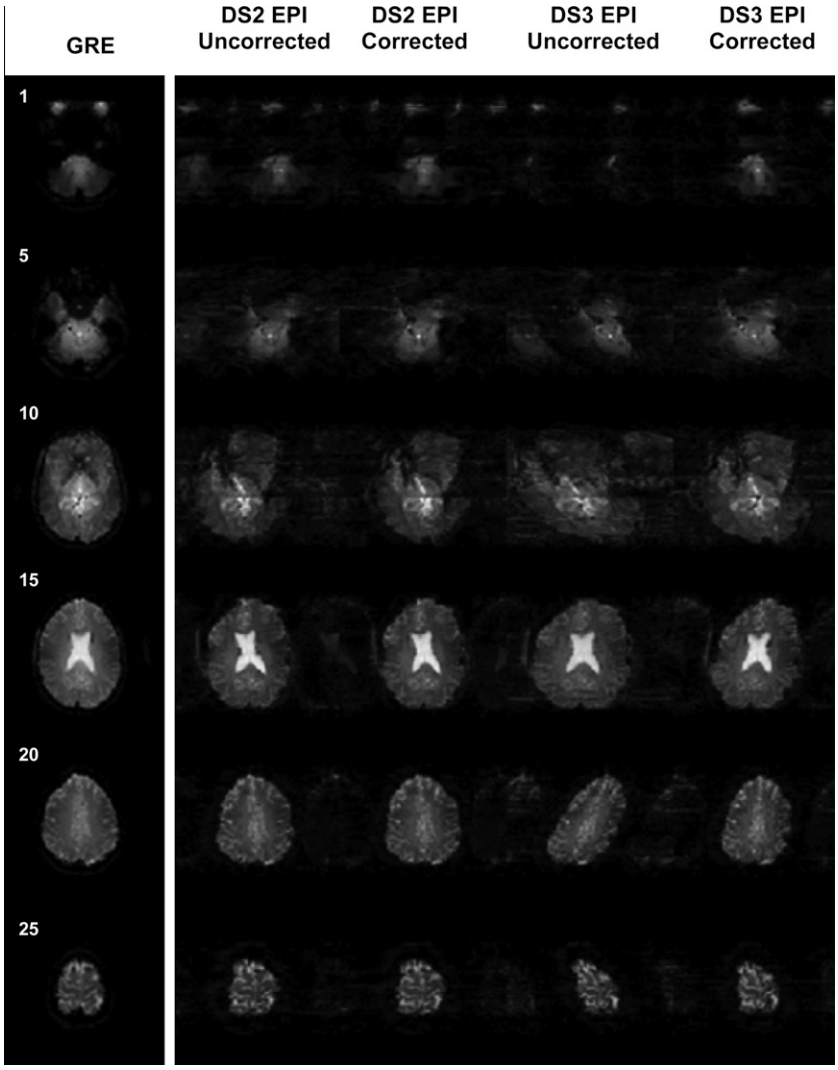

Fig. 6. Slices from 2nd and 3rd order dynamically shimmed (DS2 and DS3) single shot echo planar scans before and after steady state field corrections for the human head. Images shown are post phase offset correction for odd and even echoes. Uncorrected DS2 images show left–right bulk shifts arising from $Z2$ to $Z0$ interactions that are corrected by the method. Uncorrected DS3 images show severe distortions, bulk shifts and signal losses due to 3rd order to 1st order interactions, corrected to a large extent by the steady state corrections. No SENSE acceleration was employed. High bandwidth gradient echo images and slice numbers are shown in the left panel.

3rd order shims, the number of shim interactions increases significantly. One approach to correcting this may be to measure the individual short time constant shim step responses and using this information for correcting the data in a post processing step. Alternatively, the effects of these fields on k space may be measured in phase measurement preparation stages and partially compensated by data post processing. The long and medium time constant eddy fields and their build up are more difficult to calibrate and predict using preparation phase measurements. The steady state correction method compensates for these fields.

We have ignored the very short time constant effects of shim switches in our steady state assumptions. The very short time constants of the shim eddy currents range from less than a millisecond to a few milliseconds [4,5,11,12]. The fields with very short time constants (<1 ms) may not be included in the steady state and practically may not influence the signal, as usually a delay of ~5 ms is added after shim switching for shim amplifier settling. Alternatively, the ramp times may be extended to reduce the shortest time constant eddy currents.

This technique may not work in cases where the shims may be switched randomly where steady state is not set up, for instance in compensation of respiration induced field fluctuations. In that particular instance though, only 1st order DS or 1st order DS on top of 2nd order global shims may be sufficient.

Going further, one may be able to develop a *complete general model* of the $\boldsymbol{C}$ vector that will model the variation of $\boldsymbol{C}$ with respect to the Δt_{ss} and number of slices for a given scanner. Under normal day to day operating conditions, the correction factors are not expected to change significantly. Therefore, information from a single one time phantom calibration scan can be used to develop the general model describing the complete interaction between the shims in the system. Such a calibration scan may be for example included in a periodic quality assurance procedure to account for long term changes in the magnet's behavior. This general model may then be employed for compensation of eddy fields in any given scan.

6. Conclusion

A novel method for software based prospective compensation of eddy fields produced by dynamic shim switching has been described and demonstrated. The method is based on the assumption

of reaching an eddy field steady state generated during a dynamic B_0 shimming experiment. The static and dynamic interactions of the entire shim system are characterized and represented by a single correction factor matrix derived from a one time phantom calibration scan. The method is shown to be independent of the shim switching pattern, imaged object and the actual shim values. The method does not require expensive hardware, shim eddy current compensation or shim shielding thereby providing an economical and efficient alternative. Future work will involve developing a general model of correction factors parameterized in terms of Δt_{ss} and number of slices that will enable software eddy field correction for any multislice DS experiment.

Acknowledgments

The authors thank Adam Anderson and Chuck Nockowski for his contributions. The work was funded by NIH Grant No. RO1EB000461

References

[1] A.M. Blamire, D.L. Rothman, T. Nixon, Dynamic shim updating: a new approach towards optimized whole brain shimming, Magn. Reson Med. 36 (1996) 159–165.

[2] G. Morrell, D. Spielman, Dynamic shimming for multi-slice magnetic resonance imaging, Magn. Reson Med. 38 (1997) 477–483.

[3] R.A. De Graaf, P.B. Brown, S. McIntyre, D.L. Rothman, T.W. Nixon, Dynamic shim updating (DSU) for multislice signal acquisition, Magn. Reson Med. 49 (2003) 409–416.

[4] K.M. Koch, S. McIntyre, T.W. Nixon, D.L. Rothman, R.A. De Graaf, Dynamic shim updating on the human brain, J. Magn. Reson. 180 (2006) 286–296.

[5] C. Juchem, T.W. Nixon, P. Diduch, D.L. Rothman, P. Starewicz, R.A. de Graaf, Dynamic shimming of the human brain at 7 Tesla, Concepts Magn. Reson. Part B Magn. Reson. Eng. 37B (2010) 116–128.

[6] P. Van Gelderen, J.A. de Zwart, P. Starewicz, R.S. Hinks, J.H. Duyn, Real-time shimming to compensate for respiration-induced B0 fluctuations, Magn. Reson Med. 57 (2007) 362–368.

[7] Y. Zhao, A.W. Anderson, J.C. Gore, Computer simulation studies of the effects of dynamic shimming on susceptibility artifacts in EPI at high field, J. Magn. Reson. 173 (2005) 10–22.

[8] M. Poole, R. Bowtell, Volume parcellation for improved dynamic shimming, Magn. Reson. Mater. Phys. 21 (2008) 31–40.

[9] P. Mansfield, B. Chapman, Active magnetic screening of coils in NMR imaging, J. Magn. Reson. 66 (1986) 573–576.

[10] D. Jensen, W. Brey, J. Delayre, P. Narayana, Reduction of pulsed gradient settling time in the superconducting magnet of a magnetic resonance instrument, Med. Phys. 14 (1987) 859–862.

[11] G. Glover, N. Pelc, Method for Magnetic Field Gradient Eddy Current Compensation, US Patent #4698,591, 1987.

[12] S. Sengupta, E.B. Welch, Y. Zhao, D. Foxall, P. Starewicz, A.W. Anderson, M.J. Avison, J.C. Gore, Dynamic B_0 Shimming at 7 Tesla, in: Proc. 17th Annual Meeting ISMRM Hawaii, 777, 2009.

[13] S. Sengupta, E.B. Welch, A.W. Anderson, J.C. Gore, M.J. Avison, Software Compensation of Eddy Current Fields in Multislice Higher Order Dynamic B_0 Shimming, in: Proc. 18th Annual Meeting ISMRM, Stockholm, 1540, 2010.